BNL-223740-2022-JAAM

Conversion of CO2 to methanol and ethanol on Pt/CeOx/TiO2(110): Enabling role of water in C-C bond formation

J. Graciani, J. A. Rodriguez

To be published in "ACS Catalysis"

November 2022

Chemistry Department

Brookhaven National Laboratory

U.S. Department of Energy

USDOE Office of Science (SC), Basic Energy Sciences (BES) (SC-22)

DISCLAIMER

Conversion of CO_2 to methanol and ethanol on $Pt/CeO_x/TiO_2(110)$: Enabling role of water in C-C bond formation

*Jesús Graciani[1,3], David C. Grinter [1,2], Pedro J. Ramírez,[4,5] Robert M. Palomino [1], Fang Xu [1,6], Iradwikanari Waluyo [7], Dario Stacchiola,[1,8] Javier Fdez. Sanz[3], Sanjaya D. Senanayake [1], and José A. Rodriguez[1] **

[1] Chemistry Division, Brookhaven National Laboratory, Upton, New York 11973, USA

[2] Diamond Light Source, Didcot, Oxfordshire, OX11 0DE, United Kingdom

[3] Departamento de Química Física, Universidad de Sevilla, Sevilla 41012, Spain

[4] Facultad de Ciencias, Universidad Central de Venezuela, 1020-A Caracas, Venezuela

[5] Zoneca-CENEX, R&D Laboratories, Alta Vista, 64770 Monterrey, México

[6]Department of Chemistry, University of Texas at San Antonio, San Antonio, Texas 78249, USA

[7]National Synchrotron Light Source II, Brookhaven National Laboratory, Upton, New York 11973, USA

[8]Center for Functional Nanomaterials, Brookhaven National Laboratory, Upton, New York 11973, USA

[*] Corresponding author: Bldg. 555A, Brookhaven National Lab, P.O. Box 5000, Upton, NY 11973-5000, USA, 631-344-4343, rodrigez@bnl.gov

Abstract

The surface chemistry of alcohol synthesis from CO_2 hydrogenation has been investigated using kinetic testing, ambient pressure x-ray photoelectron spectroscopy (AP-XPS) and DFT calculations over a multicomponent system where Pt and ceria nanoparticles coexisted on a titania template, $Pt/CeO_x/TiO_2(110)$. Due to its high ability to bind and activate CO_2, not seen for typical Cu-ZnO catalysts, the Pt-CeOx-TiO_2 interface is excellent for the hydrogenation of CO_2 to methanol with some ethanol also being produced (21% selectivity). The results of AP-XPS and DFT calculations indicate that the active state involves a mixture of Ti^{4+}/Ti^{3+}, Ce^{3+} and Pt^0/Pt^+. A fast pathway for the formation of CH_3O species is only plausible when Ce^{3+} and Pt are present. The addition of water to the reaction feed facilitates the first hydrogenation of CO_2 and substantially enhances the surface coverage of C-containing species (CH_3O, HCOO, CO_3, CH_x), facilitating the formation of C-C bonds and the production of ethanol (38% selectivity).

Keywords: CO_2 hydrogenation; Methanol synthesis; Ethanol synthesis; Platinum; Ceria; Titania.

1. Introduction

The continuously rising levels of carbon dioxide (CO_2) in the atmosphere and oceans are a serious concern for the future of humanity on our planet.[1,2] As a result, there are major environmental and economic incentives to transform CO_2 into high-value chemicals or fuels.[2,3] Alcohols, such as methanol and ethanol, have proven to be promising alternative fuels due to their high energy density and compatibility with the current distribution systems. The catalyst most frequently used in the industry for methanol synthesis from $CO_2/CO/H_2$ is a $Cu/ZnO/Al_2O_3$ composite,[4,5,6] but this system requires complex activation steps, operates at relatively high pressures, suffers from severe deactivation through particle sintering, and is pyrophoric in nature.[7,8] Thus, a search for a more stable and active catalyst that is also capable of producing higher alcohols and oxygenates, such as ethanol, directly from CO_2/H_2 feeds is crucial.[8,9]

The surface processes that lead to CO_2 hydrogenation to alcohols require several key steps, involving initially the adsorption of both CO_2 and H_2, followed by the activation of each reactant.[8,9,10] CO_2 upon complete activation forms adsorbed CO_3, CO and O, which are then hydrogenated using atomic H coming from a H-H bond scission. This step where H adatoms are incorporated into a H_xCO_y species can lead to several carbonaceous species including methoxy (CH_3O), formate (HCOO) or carboxylates (H_yCO_x).[3,8,9] However, at this point any chance of C-C bond formation (to make C_2 or C_n oxygenates) must further rely on the coupling of hydrogenated adsorbates, which is a difficult process. A promoter like Cs facilitates the coupling of HCO fragments on Cu/ZnO and the generation of ethanol.[10] However, the selectivity towards ethanol formation from pure CO_2 hydrogenation is limited.[10] In this work, we have found that a significant yield (10-15%) of the C_2 alcohol can be obtained when using $Pt/CeO_2/TiO_2(110)$ as a catalyst. Our Pt-

CeO_x-TiO_2 interface alone can generate ethanol from a CO_2/H_2 feed and its yield increases when water is added to the CO_2/H_2 reaction feed.

Recent studies have shown that a $Pt/CeO_2/TiO_2$ system has a unique ability to bind and activate the CO_2 molecule not seen in the case of Pt/TiO_2 and Pt/CeO_2 surfaces.[11] Ceria wires and nano structures in contact with titania display structural and electronic properties not observed for bulk ceria.[12,13] The results of theoretical calculations based on density-functional theory (DFT) showed that a $Pt/CeO_x/TiO_2(110)$ surface binds CO_2 much more strongly than surfaces of bulk platinum {(111), (100), (110)} or other late transition metals.[11] On a Pt-CeO_x-TiO_2 interface, the molecule adsorbs with a bent configuration (~ 130^o O-C-O bond angle) and with a substantial elongation (~ 0.1 Å) of the C-O bonds, facilitating its transformation into high value chemicals.[11] In this work, we carefully probe the reaction mechanisms under CO_2/H_2 and $CO_2/H_2/H_2O$ feeds using *in situ* characterization with X-ray photoelectron spectroscopy (XPS) and DFT calculations. Ambient-pressure (AP) XPS spectra obtained under different process conditions are employed to elucidate not only the chemical and electronic structure of the catalyst active components, but the possible reaction intermediates as well. The results of the AP-XPS measurements and the DFT calculations point to new concepts for the design of better catalysts in the conversion of CO_2 to higher alcohols.

2. Methods

2.1 Surface characterization, photoemission, and catalytic studies

The rutile $TiO_2(110)$ surfaces utilized in this study were cleaned and bulk reduced by combining ion sputtering with Ar^+ and subsequent annealing at 950 K until the graphitic carbon peak in the C 1s XPS region was removed and small Ti^{3+} peaks appeared in the Ti

2p XPS region as a consequence of the creation of O vacancies. CeO_x nanoparticles were dispersed on the titania by evaporating ~0.1 monolayer equivalents (MLE) of Ce onto the oxide substrate at 300 K under an O_2 pressure of 3×10^{-7} Torr followed by annealing in the same O_2 background to 800 K. [12,13] Finally, 0.2 MLE of Pt were deposited from a high-purity platinum rod onto the $CeO_x/TiO_2(110)$ substrate at room temperature in ultrahigh vacuum (UHV) conditions, with subsequent heating to a temperature of 700 K.[11,12] The Ce and Pt coverages were determined using a quartz crystal microbalance.

Scanning Tunneling Microscopy (STM) imaging was carried out at 300 K on an Omicron VT-STM system under UHV conditions ($\sim 5 \times 10^{-10}$ Torr) using etched W tips.[12,13] The ambient pressure X-ray photoelectron spectroscopy (AP-XPS) studies were performed using the AP-PES end-station of the IOS (23-ID-2) beamline within the National Synchrotron Light Source II (NSLS-II). A differentially pumped SPECS electrostatic analyzer was used in these measurements. The XPS spectra were recorded in a wide range of pressures (from UHV to < 2 Torr) employing a 300 μm aperture cone and a differentially pumped analyzer. This set-up allowed the detection of electrons at ambient pressure while maintaining the analyzer under near UHV.[11] The sample electrons were excited using the following photon energies: 1200 eV (Ce 3d), 888 eV (valence band on-resonance for Ce 3d-4f), 750 eV (C1s, Ti 2p, O 1s, Pt 4f), and 460 eV (valence band on-resonance for Ti 2p-3d), with an overall energy resolution of 0.4-0.5 eV. In general, spectra were collected on the clean TiO_2 system under UHV, 100 mTorr CO_2, 900 mTorr H_2, and 100 mTorr CO_2 + 900 mTorr H_2 at 300 and 473 K. These systematic measurements were replicated after ceria deposition on the titania, and again upon addition of the platinum. For the energy

calibrations, we used alignment of the spectra to both the Fermi level and the signal of adventitious hydrocarbon species.[11]

A set-up that combined an UHV chamber for surface characterization and a batch micro-reactor for catalytic tests was used in the experiments measuring the catalytic activity of the different examined systems.[10,12,13,14] Instrumentation for XPS (Al/Mg K alpha), temperature programmed desorption (TDS), and ion-scattering spectroscopy (ISS) was available in the UHV chamber.[10,12-14] Following previous works,[3,8,9,15,16] the catalytic hydrogenation of CO_2 was examined at temperatures between 500 and 600 K. After initial characterization in the UHV chamber, the $Pt/CeO_2/TiO_2(110)$ surfaces were transferred to the batch reactor at room temperature, the reactant gases were added {0.049 MPa (0.5 atm) of CO_2 plus 0.441 MPa (4.5 atm) of H_2}, and finally the samples were rapidly heated to the desired reaction temperature.[10,14-16] A combination of mass spectroscopy and gas chromatography was used to follow the variations in the gas composition inside the reactor, [15,16] with data collection at intervals of 10 to 15 minutes for up to 12 hours. The production of CO, methanol, and ethanol in the catalytic tests was normalized by the surface area exposed by each catalyst sample and the total reaction time. All the kinetic experiments with the different catalysts {Pt(111), $Pt/TiO_2(110)$, $Pt/CeO_2(111)$ and $Pt/CeO_x/TiO_2(110)$} were done in the limit of low conversion (<5%).

2.2 Density functional calculations

The DFT calculations were carried out following the plane-wave-pseudopotential approach within the projector augmented wave method (PAW)[17,18] utilizing the GGA exchange correlation functional developed by Perdew *et al.*[19] (PW91) and the algorithms of the VASP code.[20,21] The calculations were performed with a plane-wave cutoff energy

of 400 eV, treating the Ti (3*s*, 3*p*, 3*d*, 4*s*), Ce (4f, 5*s*, 5*p*, 5*d*, 6*s*), Pt (5*d*, 6*s*) and O (2*s*, 2*p*) electrons as valence states, while the remaining electrons were kept frozen as core states. To accelerate the convergence, thermal smearing of one-electron states (k_BT = 0.05 eV) was allowed employing the Gaussian smearing method to define the partial occupancies. All the energies were evaluated at the gamma point.

The model used to describe the $Pt/CeO_x/TiO_2(110)$ catalyst was previously employed to examine CO_2 chemisorption and activation on this surface.[11] It has ceria diamers and a Pt_{10} particle (0.8 nm in diameter).[11] The model contains the basic features observed in STM images for the $Pt/CeO_x/TiO_2(110)$ system,[12,13] where the ceria is present as surface dimers and the Pt forms aggregates that range in size from clusters with a few atoms to particles with a size below 1 nm. A (6×2) surface model was selected with the aim of having isolated CeO_x dimers and a Pt_{10} particle on the TiO_2 (110) substrate. The used slab had a thickness of 12 atomic layers or four TiO_2-trilayers, as it was verified that thicker supercell models gave similar results.[22] In our calculations, the two lower TiO_2 trilayers remained frozen while the rest of the atoms in the slab were allowed to fully relax their atomic positions. In the supercell, a vacuum of 15 Å was used to separate the slabs, being enough to avoid slab-slab interactions. The optimized lattice parameters for bulk titania {a = 4.1616 Å, c = 2.974 Å, and u = 0.304 Å} were employed for building the supercell model. This type of model has been successfully used in previous works examining the chemical and catalytic properties of $metal/CeO_x/TiO_2(110)$ systems and provides the key features of metal-ceria-titania interfaces.[11,12,23]

A GGA+*U* formalism was used to represent adequately the electronic structure of Ce (in particular the 4*f* level of the Ce^{3+} species). The Hubbard *U* term was added to the plain

GGA functional employing the rotationally invariant approach proposed by Dudarev et al.,[24] where the Coulomb U and exchange J parameters are combined into a single parameter $U_{eff} = U\text{-}J$. A U_{eff} of 4.5 eV was used for Ce, a value self-consistently calculated by Fabris et al.[25] following the linear-response approach of Cococcioni and de Gironcoli.[26] This U_{eff} of 4.5 eV is in the range of values usually proposed in the literature (4.5-5.5 eV) for GGA+U calculations.[27,28,29,30,31,32,33,34,35] In the case of the Ti 3d states, a U_{eff} parameter of 4.5 eV was also used because it reproduces the experimental values of the gap between the Ce^{3+} 4f and Ti^{3+} 3d levels observed in valence photoemission spectra for the $Ce/TiO_2(110)$ surface.[13] In the literature, lower values for U_{eff} have been suggested for a balanced description of bulk CeO_2 and Ce_2O_3 oxides,[36,37] but the set of parameters we have chosen gives a correct description of the gaps observed in the experimental photoemission spectra of our systems consisting of CeO_x clusters supported on the $TiO_2(110)$ substrate.[12,13] The existence of Ce^{3+} cations was shown by a characteristic 4f peak in the band gap and subsequently verified by the magnetization of the Ce atoms (> 0.9 electrons) observed in the calculations. Similarly, a clear 3d peak in the band gap indicated the presence of Ti^{3+} species and this was later confirmed by the magnetization of the Ti atoms (>0.8 electrons) seen in the calculations. These U_{eff} parameters for Ce and Ti have been used successfully in previous studies involving $CeO_x/TiO_2(110)$ systems. [11,12,13,23,38]

In this work, transition states for CO_2 hydrogenation were calculated utilizing the climbing image version of the nudged elastic band (NEB) algorithm,[39] and in all cases, after a vibrational analysis, only one imaginary frequency has been obtained for these structures.

3. Results

3.1 Characterization of the model catalyst: STM and XPS studies

The surface of the Pt/CeO_x/TiO_2(110) system was initially characterized using imaging (STM) and spectroscopy (XPS) thoroughly upon preparation prior to any experimentation with reactants.[11,12,13] In previous works examining the behavior of metal/CeO_x/TiO_2(110) surfaces, it was found that active metal-ceria-titania interfaces were found only when co-adsorbing small amounts of the metal and ceria on titania.[12,13,23,40] At large coverages, big particles of the metal or ceria were seen, most of the atoms were not in a metal-ceria-titania interface, and a substantial drop in catalytic activity occurred.[12,13,23,40] Furthermore, to reduce costs, it is also desirable to reduce the amount of Pt and ceria in the catalyst. Thus, in this work, we focused on a system were 0.1 ML of ceria and 0.2 ML of Pt coexisted on TiO_2(110) template.

Figure 1 shows STM images for the CeO_x/TiO_2(110) and Pt/CeO_x/TiO_2(110) surfaces. Low coverages of ceria on TiO_2(110) have been investigated previously[12,13] and are characterized by CeO_x dimers (green square highlight) and other small clusters located on the Ti_{5c} rows (bright lines along [001] in the STM images) as well as (2 × 1) reconstructed regions of TiO_2(110) resulting from partial reduction of the surface (grey rectangle highlight). The low density of point defects on the TiO_2(110) surface is due to the oxidation process that occurs when forming CeO_x particles. After deposition of Pt and annealing to ~600 K, bright Pt nanoparticles (blue circle highlight) are observed. They are evenly distributed across the CeO_x/TiO_2 surface and in close contact with the CeO_x dimers and the TiO_2 surface. From the line profile shown in Figure 1, Pt forms particles ~0.5 nm

tall (their width is exaggerated by tip-convolution effects), in comparison to the CeO_x dimers which are ~0.1 nm high above the TiO_2.

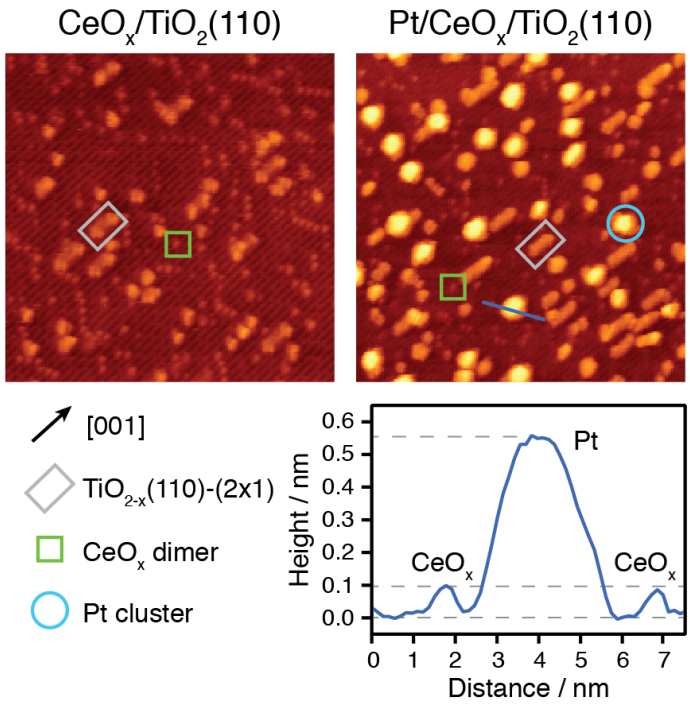

Figure 1: STM images of the low coverage $Pt/CeO_x/TiO_2(110)$ catalyst. (35 × 35 nm^2, +1.21 V, 0.05 nA).

The $Pt/CeO_x/TiO_2(110)$ catalyst was characterized by XPS in UHV (Figure S1).[11] Initially, before the deposition of CeO_x and Pt, the clean $TiO_2(110)$ surface was partially reduced, with ~15% Ti^{3+} species according to the Ti 2p spectrum. After deposition of CeO_x and annealing in O_2, the $TiO_2(110)$ surface appeared more oxidized (< 5% Ti^{3+}) and the CeO_x remained as mainly Ce^{3+} with only a small amount of fully oxidized species (~ 30% Ce^{4+}). After the addition of Pt to the $CeOx/TiO_2(110)$ surface, the Ti 2p and Ce 3d regions showed little change in oxidation state (Figure S1).[11] In principle, the $Pt/CeO_x/TiO_2(110)$ system exposes ceria dimers that can be very useful for the activation of O-containing molecules and Pt clusters that can be active in hydrogenation processes.[11,12]

3.2 Hydrogenation of CO_2 to alcohols on $Pt/CeO_x/TiO_2(110)$: Effects of water

In a set of studies, we investigated the hydrogenation of CO_2 on a series of surfaces that exposed Pt sites in different configurations and supports, Figure 2. The experiments were done using CO_2/H_2 (blue bars) and $CO_2/H_2/H_2O$ (grey bars) reaction mixtures. Under dry conditions, the main product of the hydrogenation process was CO with methanol as a secondary product. Pure Pt(111) displayed a rather low activity due to the deposition of carbon probably coming from the full decomposition of CO_2 to CO and finally C. Metal-support interactions can reduce the tendency of Pt to dissociate CO.[40] Upon the deposition of Pt on $TiO_2(110)$ and $CeO_2(111)$, there was a significant increase in the catalytic activity for methanol production, but by far the best catalyst was $Pt/CeO_x/TiO_2(110)$. When using the metal loading per unit of area as reference, this system displays a catalytic activity that is larger (1.6-2.8 times) than that seen under the same conditions for Cu/ZnO catalysts.[10,14] Furthermore, among the systems displayed in Figure 2, $Pt/CeO_x/TiO_2(110)$ was the only catalyst that was able to produce a minor amount of ethanol (~ 21% selectivity with respect to the amount of methanol formed). This is probably a consequence of the special chemical properties of the Pt-CeO_x-TiO_2 interface.[11] Neither Cu/ZnO nor ZnO/Cu produced ethanol under the same CO_2 hydrogenation conditions.[10,14]

The experiments in Figure 2 were done after coadsorbing 0.1 ML of ceria and 0.2 ML of Pt on the $TiO_2(110)$ substrate. Experiments were also performed for 0.3 and 0.4 ML of Pt on the $CeO_x/TiO_2(110)$ surface, showing 17% and 31% drops in the conversion of CO_2 to alcohols (respectively). This reduction in the catalytic activity is probably a consequence of an increase in the size of the Pt particles,[12,13,40] since many of the metal

adatoms were not part of a platinum-ceria-titania interface. In this aspect, the system in Figure 2 has an optimal composition.

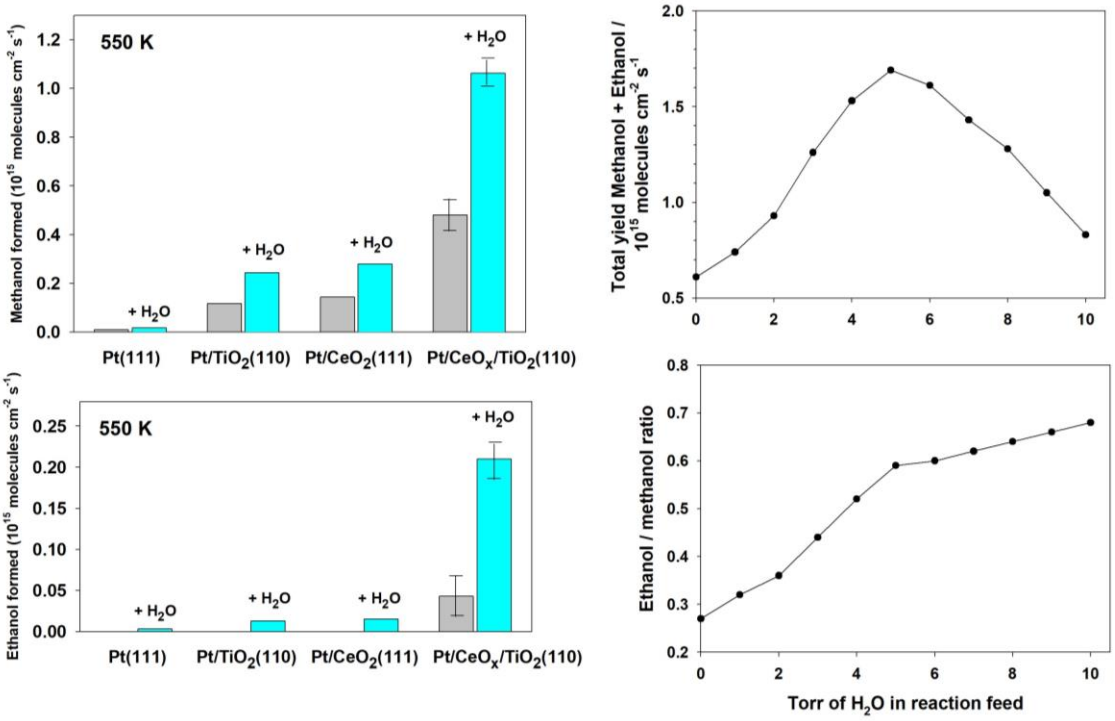

Figure 2 Rates measured for the production of methanol and ethanol on Pt(111), $Pt/TiO_2(111)$, $Pt/CeO_2(111)$, and $Pt/CeO_x/TiO_2(110)$. The amount of Pt present on the oxide supports was 0.2 MLE. The $Pt/CeO_x/TiO_2(110)$ system contained 0.1 MLE of CeO_x. Reaction conditions: T= 550 K, P_{H2}= 4.5 atm, P_{CO2}= 0.5 atm. The experiments were performed without (blue bars) and with water (grey bars, + 5 Torr of H_2O). The right-side of the figure shows the effect of water on the methanol + ethanol yield and on the ethanol/methanol ratio.

It is known that $CeO_x/TiO_2(110)$ and $Pt/CeO_x/TiO_2(110)$ are very reactive towards water.[12,38] On $CeO_x/TiO_2(110)$, the calculated energy barrier for the dissociation of a H-OH bond is only 0.04 eV.[38] We found that the addition of small amounts of water to the reaction feed induced big changes in the activity of the $Pt/CeO_x/TiO_2(110)$ catalyst towards methanol and ethanol production. For all the catalysts investigated, the presence of water

had a positive effect enhancing the rate of methanol formation. In the case of $Pt/CeO_x/TiO_2(110)$, there was a simultaneous increase in the formation of methanol and ethanol, but the selectivity towards the higher alcohol (~ 38%) was almost double in the presence of water.

In principle, the extra water could have modified the properties of the catalyst surface by hydroxylation[12,38] or perhaps provided OH groups that participated directly in the generation of alcohol molecules. Both possibilities will be tested below using DFT calculations. It is important to mention that the addition of too much water did have a negative effect. In the experiments of Figure 2, when the amount of water added to the reaction feed was larger than 5 Torr, we saw an overall drop in the conversion of CO_2 and the production of methanol and ethanol. Thus, surface sites involved in the activation of CO_2 were removed by water blocking or surface morphological changes.[41,42,43] Post-reaction characterization with XPS showed that these catalysts displayed a large signal around 531.5 eV in the O 1s region that could be attributed to adsorbed OH groups typically found after dosing water to $CeO_x/TiO_2(110)$ and $Pt/CeO_x/TiO_2(110)$.[12,38]

3.3 Surface chemistry of CO_2 hydrogenation: AP-XPS studies on the role of water

In a previous study, using AP-XPS and DFT calculations, we were able to show that a $Pt/CeO_x/TiO_2(110)$ system is very effective for the binding and activation of CO_2 (Figure S2).[11] This is a remarkable property of $Pt/CeO_x/TiO_2(110)$ not seen in Cu-ZnO catalysts or for plain Pt surfaces.[10,14,15,44] Figure 3a compares C 1s XPS spectra collected while exposing a $Pt/CeO_x/TiO_2(110)$ surface to mixtures of CO_2/H_2 (bottom trace) and $CO_2/H_2/H_2O$ (top trace). Dosing of CO_2 or a CO_2/H_2 mixture to $TiO_2(110)$ and $CeO_x/TiO_2(110)$ only produced a C 1s feature at ~ 290 eV (Figures S2 and S3) that can be

attributed to adsorbed carbonate (CO_3) or formate (HCOO) species on the basis of previous studies of XPS, NEXAFS and vibrational spectroscopy.[45,46] In Figure 3, a rich chemistry is seen after exposing the $Pt/CeO_x/TiO_2(110)$ system to CO_2/H_2 and $CO_2/H_2/H_2O$ mixtures. The results in the figure are representative of many experiments. The major surface species are adsorbed CO_3/HCOO (290 eV),[45,46] CH_3O (287 eV),[47,48,49,50] and CH_x (284.5 eV)[46,50] groups. These species already have been detected in previous studies of CO_2 hydrogenation or methanol decomposition using XPS in combination with other surface science techniques.[45-51] The coverages of these C-containing groups on the $Pt/CeO_x/TiO_2(110)$ catalyst were not large (< 0.35 ML), being frequently small (< 0.1 ML), see Figure 3b.

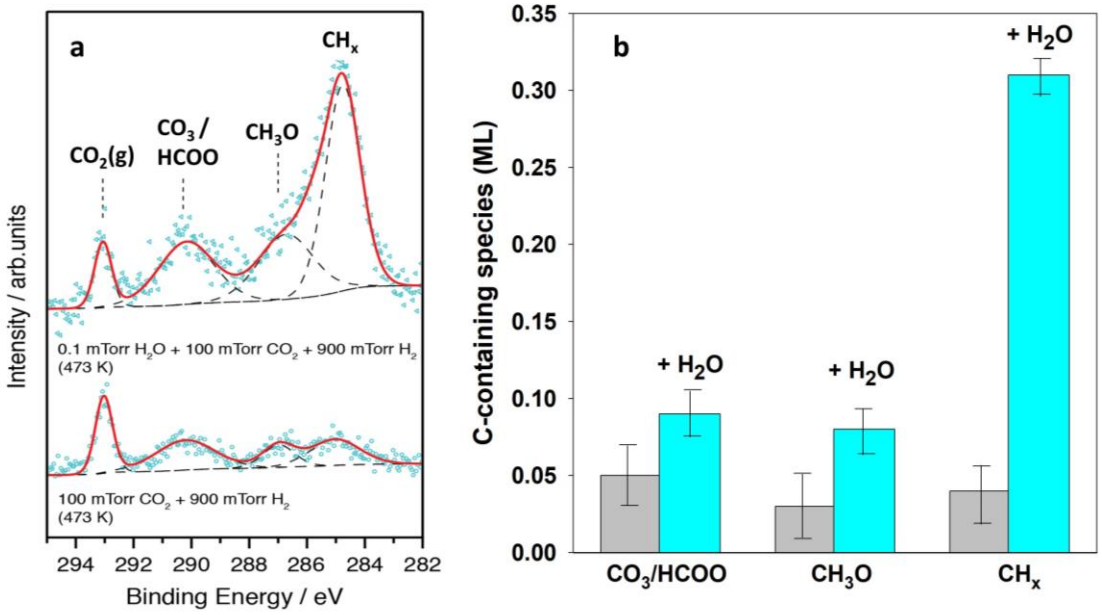

Figure 3. (a) C 1s XPS spectra of $Pt/CeO_x/TiO_2(110)$ at 473 K under 0.1 mTorr H_2O + 100 mTorr CO_2 + 900 mTorr H_2 (top) and 100 mTorr CO_2 + 900 mTorr H_2 (bottom). (b) Effect of water on the coverage of C-containing species adsorbed on the $Pt/CeO_x/TiO_2(110)$ catalyst during CO_2 hydrogenation at the conditions of part (a).

These observations suggest that the TiO_2 and CeO_x components adsorbs CO_2 by forming surface carbonates (CO_3), consistent with previous studies on the individual oxides,[45,52] while the Pt facilitates the H insertion into adsorbed CO_2 to form CH_3O, HCOO and CH_x surface species. Our DFT calculations (to be described below) confirm this interpretation. The CO_2 hydrogenation chemistry occurs through a synergy between all parts of this catalyst including both Pt and CeO_x contributing towards a multi-functional mechanism.

In Figure 3, one sees substantial differences for the adsorbed species with very intense CH_x (284.2 eV) features and some additional HCOO (290 eV) and CH_3O (286.5 eV) when comparing the spectra for dry and wet conditions. The total coverage of C-containing species (CO_3, HCOO, CH_3O, CH_x) clearly increased under the $CO_2/H_2/H_2O$ mixture. This enhancement is quite important since HCOO and CH_3O are precursors for the production of methanol [2,8,9,15] and the CH_x groups are necessary for C-C bond formation and the generation of ethanol.[8]

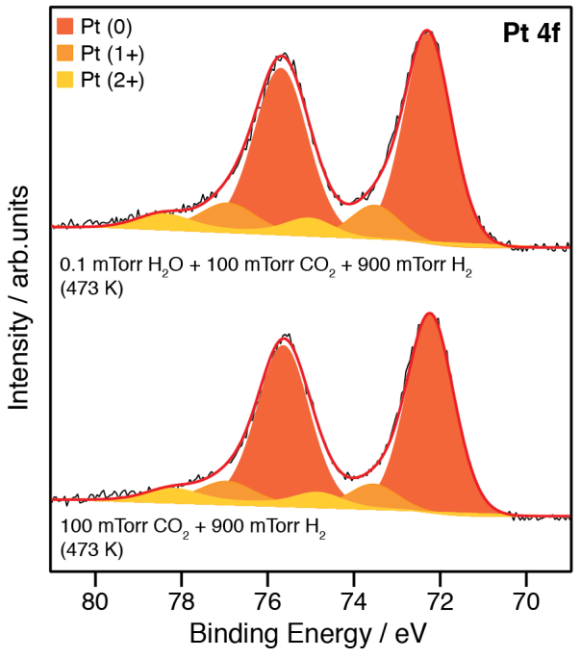

Figure 4. Pt 4f XPS spectra of $Pt/CeO_x/TiO_2(110)$ at 473 K under 0.1 mTorr H_2O + 100 mTorr CO_2 + 900 mTorr H_2 (top) and 100 mTorr CO_2 + 900 mTorr H_2 (bottom).

Figure 4 compares the Pt 4f spectra of a $Pt/CeO_x/TiO_2(110)$ catalyst with and without the presence of water. In both cases, curve fitting showed mainly Pt^0 with some additional peaks that could come from Pt^{1+} and Pt^{2+} on the surface.[11,40] Even in the presence of pure H_2, the Pt^{1+} and Pt^{2+} species were not fully reduced (Figure S4). This may be a consequence of strong metal-support interactions as we will see bellow in our DFT studies. In the experiments of Figure 4, the reducing environment associated with the presence of hydrogen prevented a major oxidation of Pt^0 by water and there was only a small increase in the coverage of Pt^{1+}.

3.4 Active sites and reaction mechanism: DFT studies

On the basis of previous work,[11] to represent the $Pt/CeO_x/TiO_2(110)$ catalyst, we used a slab where CeO_x dimers and a Pt_{10} metal cluster (0.8 nm in diameter) coexisted on

a TiO_2 (110) substrate. The Pt_{10} cluster is within the range of Pt species seen in the STM studies (Figure 1 and refs 12 and 13) and it allows the creation of a platinum-ceria-titania interface where the chemistry can take place.[11] In this respect, the inclusion of the CeO_x dimers is essential to properly describe the behaviour of the metal/CeO_x/TiO_2(110) system.[11,12,23,38] Our DFT calculations confirm the oxidation states experimentally observed. The Ce^{3+} is due to the observed dimers stoichiometry (Ce_2O_3), while there is a charge transfer from the Pt clusters to TiO_2, generating some Pt^+ and Ti^{3+} species (see Discussion 1 in Supporting Information).

A. Activation of CO_2 at the Pt-CeO_x interface in the Pt/CeO_x/TiO_2(110) system

The adsorption of CO_2 on TiO_2(110) has been extensively studied from both experimental and theoretical points of view. It is a weak interaction with desorption temperatures between 110 and 166 K.[53] However, our C 1s XPS results exposing TiO_2(110) to 100 mTorr CO_2 at 473 K (Figure S2) show the formation of CO_3-like species under those conditions. To elucidate this point, we studied the adsorption of CO_2 in its most stable site of the surface and its further transformation in CO_3 by interaction with a bridging oxygen of the surface. The calculated adsorption energy is -0.47 eV (very close to the experimental values ~0.5 eV). The formation of CO_3-like species is slightly exothermic by only -0.05 eV, with a low energy barrier of 0.25 eV (Figure 5). Therefore, under the current experimental conditions, CO_3-like species are expected on the TiO_2(110) surface after CO_2 adsorption on O sites (as seen in Figure S2).[11,52]

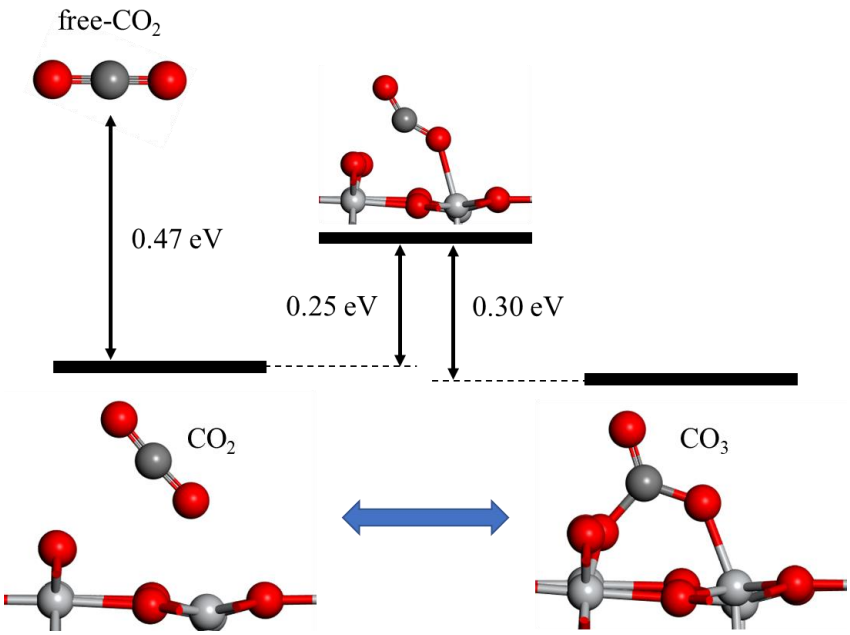

Figure 5. Optimized structures for CO_2 adsorption on TiO_2(110) and its transformation into a CO_3-like species. The involved energies and the structure of the transition state are also shown. Color code: gray (Ti), red (O), dark gray (C).

The C 1s XPS signal of these CO_3-like species (Figure S2) grows when passing from pure TiO_2(110) to CeO_x/TiO_2(110) indicating a stronger interaction. Finally, in the system $Pt/CeO_x/TiO_2$(110) the interaction is even stronger leading not only to the formation of CO_3-like species but also to other CH_3O and CH_y species when H_2 is present, pointing to a richer chemistry. We have performed some DFT calculations to support these observations. We start by computation of the interaction energy of CO_2 with the system defined as:

$$\Delta E_{int} = E(CO_2 - System) - E(CO_2) - E(System)$$

Where System represents either TiO_2(110), CeO_x/TiO_2(110) or $Pt/CeO_x/TiO_2$(110); $E(CO_2 - System)$ is the total energy of the System after the CO_2 adsorption; $E(CO_2)$ is

the total energy of an isolated CO_2 molecule; and $E(System)$ is the total energy of each system without CO_2.

We have found that the interaction of CO_2 with the bridging oxygens of the $TiO_2(110)$ surface may lead to the formation of a CO_3 species (Figures 5 and 6a) with a total interaction energy of -0.52 eV. A similar phenomenon is observed when CO_2 interacts with an oxygen atom of the CeO_x species of the $CeO_x/TiO_2(110)$ system (Figure 6b) but with a much higher interaction energy (-1.17 eV). This certainly confirms the higher interaction that can be inferred from the experimental C 1s XPS results. More interestingly, when we tried to form the same CO_3-like species at the Pt/CeO_x interface (Figure 6c) the interaction was much lower (-0.08 eV). Such interface hindered the formation of these intermediates, fostering instead the adsorption of a CO_2 molecule at the interface as shown in Figure 6d. The interaction energy in this configuration is much larger: -1.48 eV. The C atom of the molecule interacts with Pt while both O atoms of the molecule interacts with two Ce atoms of the Ce_2O_3 particle. Where a Pt/CeO_x interface is formed on $TiO_2(110)$, the CO_3-like species are shifted to a highly activated CO_2 species ready to further reaction. Obviously, not all the cerium particles CeO_x in the $Pt/CeO_x/TiO_2(110)$ are in direct contact with Pt forming such interface. Those isolated CeO_x dimers continue interacting strongly with CO_2 to form CO_3-like species. That is why the C 1s XPS signal of CO_3-like species (Figure S2) remains in $Pt/CeO_x/TiO_2(110)$ system and coexists with other C signals, pointing to an interesting chemistry we will see below.

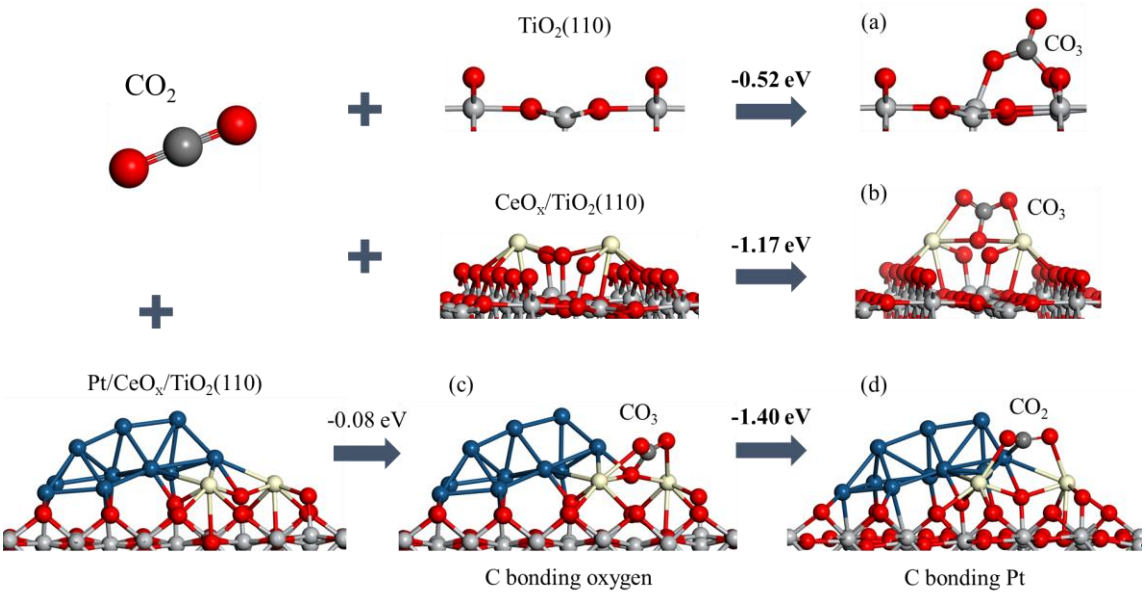

Figure 6. Optimized structures and CO_2 interaction energies to form CO_3-like species on (a) $TiO_2(110)$, (b) $CeO_x/TiO_2(110)$, and (c) $Pt/CeO_x/TiO_2(110)$; and to form CO_2 adsorbed on (d) $Pt/CeO_x/TiO_2(110)$. Color code: gray (Ti), red (O), dark gray (C), blue (Pt), crème white (Ce). Although the process depicted in (a) has been detailed in figure 5, it is shown also here for a direct comparison of the three intermediates formed by CO_2 adsorption.

B. Selecting a reaction mechanism over the $Pt/CeO_x/TiO_2(110)$ system

We are investigating reactions to form alcohols from CO_2 and H_2, according to the general formula:

$$nCO_2 + 3nH_2 \rightarrow CH_3(CH_2)_{n-1}OH + (2n-1)H_2O$$

According to our experimental results, we will deal with the first two equations of the series (n=1, methanol; n=2, ethanol):

$$CO_2 + 3H_2 \rightarrow CH_3OH + H_2O$$

$$2CO_2 + 6H_2 \rightarrow CH_3CH_2OH + 3H_2O$$

There are some reaction mechanisms proposed in the literature for *metal/oxide catalysts*.[3,7,8] All of them involve the adsorption and activation of the CO_2 molecule usually

at the metal-oxide interface, where the C atom would be adsorbed to the metal and one O atom would be adsorbed to one cation of the oxide. On the other hand, all of them assume the adsorption-dissociation of H_2 to form hydroxyls. These steps would be represented as:

$$3 * + CO_2\ (g) + H_2\ (g) \rightarrow CO_2* + 2\ H*$$

Where * stands for either a site of the surface free for adsorption or indicates that the molecule/atom is adsorbed on the surface (Figure 7a).

One of the mechanisms would go through the *formate* intermediate (O-CH-O). In this case the first step after H_2 adsorption-dissociation and CO_2 adsorption would be the hydrogenation of the C atom. In this mechanism the formate molecule is usually adsorbed to the cations of the oxide through the two oxygen atoms of the molecule (bidentate) and the C atom is not linked to either the metal or the oxide (Figure 7c). Then, a dissociation of one C-O bond would lead to the formation of *formyl* (HCO) and one O atom.

A second mechanism suggests that the reaction goes through the *formic acid* intermediate (O-CH-OH) which would come from a double hydrogenation of the CO_2 molecule: the hydrogenation of the O atom to form carboxyl (O-C-OH) and the subsequent hydrogenation of the C atom to give finally the formic acid (O-CH-OH). This intermediate is usually adsorbed to the cations of the oxide through a single oxygen atom (monodentate) or through both oxygen atoms (bidentate) and the C atom is not bound to the metal or the oxide (Figure 7d). The following step would be the dissociation of the formic acid to give *formyl* (HCO) and hydroxyl (OH).

Finally, a third mechanism points to the *carboxyl* intermediate (O-C-OH) adsorbed at the metal-oxide interface, where the C atom would be adsorbed to the metal and one oxygen atom to a cation of the oxide (Figure 7b). In this case the dissociation of the

carboxyl intermediate would lead to the formation of *carbon monoxide* (CO) adsorbed on the metal and hydroxyl (OH) adsorbed on the oxide. Therefore, this mechanism would involve the so-called *Reverse Water Gas Shift* reaction (RWGS).

In our system, we have calculated the formation energies of the three key intermediates taking as reference the energy of the system with CO_2 and 2 H atoms adsorbed forming two hydroxyl groups on the oxide:

$$CO_2* + 2\ H* \rightarrow O\text{-}C\text{-}OH* \text{ (carboxyl)} + H*$$

$$CO_2* + 2\ H* \rightarrow O\text{-}CH\text{-}O* \text{ (formate)} + H*$$

$$CO_2* + 2\ H* \rightarrow O\text{-}CH\text{-}OH* \text{ (formic acid)}$$

The energies of these processes are all endothermic with values of 0.15, 0.98 and 1.25 eV for *carboxyl*, *formate* and *formic acid*, respectively (Figure 7). The carboxyl group clearly is the more likely intermediate to form on the $Pt/CeO_x/TiO_2(110)$. The reason for this behavior is the well-known strong C-Pt bond. All the mechanisms that involve dissociation of the C-Pt (as in formate and formic acid) are energetically hindered. Therefore, we choose a methoxy and methanol/ethanol formation mechanism going through the carboxyl intermediate which keeps the C-Pt bond throughout the way.

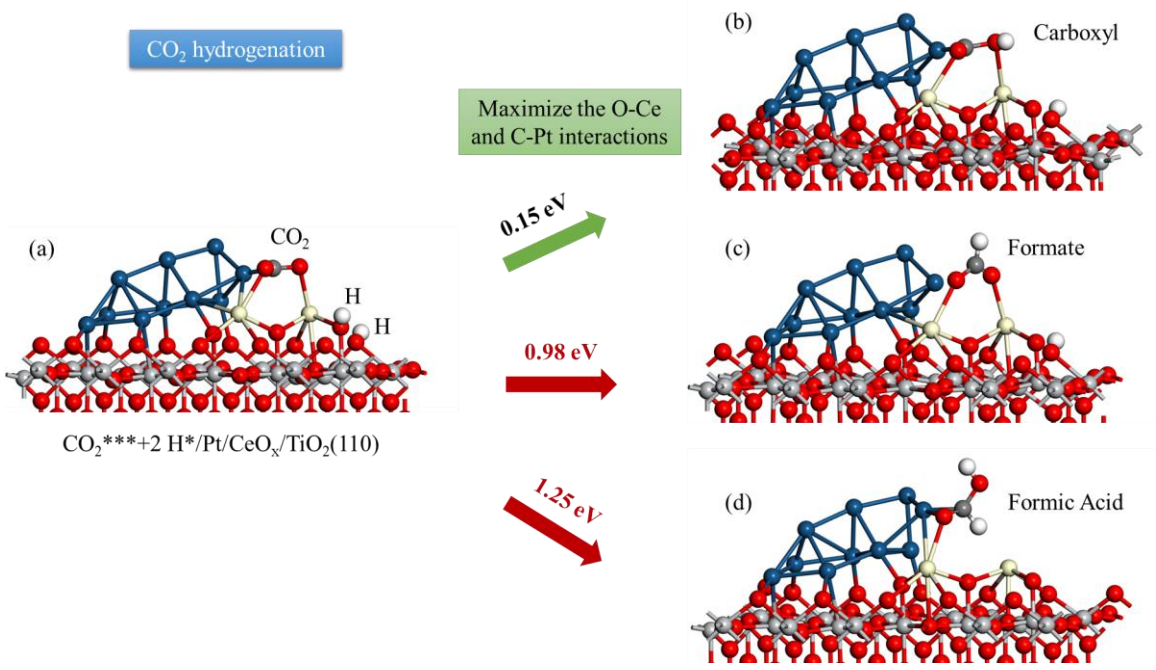

Figure 7. Optimized structures and CO_2 hydrogenation energies to form (b) carboxyl, (c) formate and (d) formic acid species on CO_2***+2H*/Pt/CeO_x/TiO_2(110). The * indicate the number of bonds to the system that the adsorbed species form. Color code: gray (Ti), red (O), dark gray (C), blue (Pt), crème white (Ce), white (H).

C. Water increases the CO_2-support interaction and strongly facilitates the first CO_2 hydrogenation

One of the most interesting results of this work is the profound effect of the water presence on the activity/selectivity of the catalyst to form methanol/ethanol. We will try to shed some light on this behavior from theoretical modeling. The first step in the alcohol synthesis from CO_2 and H_2 is critical since it involves the activation of a highly stable molecule: CO_2. Although the interaction of CO_2 with the Pt/CeO_x/TiO_2(110) system at the Pt/CeO_x interface is strong (-1.48 eV) acquiring an activated bent configuration, the presence of a water molecule dramatically increases the strength of that interaction to -2.08

eV. Such amount of energy liberated at the very beginning of the reaction boosts the evolution to products through the following steps.

A second observation helps to explain the beneficial presence of water for the activity. As indicated above, in our system, the mechanism going through carboxyl intermediate is the most likely. Once CO_2 molecule is adsorbed-activated, it must be hydrogenated to form a carboxyl (O-C-OH) group. Thus, the next key step is the adsorption-dissociation of H_2. Theoretical studies have found that the process is complicated on the oxide, with an energy barrier of around 1 eV.[54,55] In contrast, the process on Pt is almost barrierless.[56,57] Therefore, the best way to adsorb-dissociate H_2 in our system is on the Pt particle. The CO_2 hydrogenation with H coming from Pt has a high barrier of 0.95 eV. However, if there is a water molecule co-adsorbed, the transition state is strongly stabilized and the barrier for the CO_2 hydrogenation drops to half: 0.50 eV. The presence of water makes much easier the first hydrogenation of CO_2 to give carboxyl (O-C-OH).

D. Water fosters the *formation* of CH_3O* species at the Pt/CeO_x interface and its *deoxygenation* to form CH_3* species on Pt.

According to the carboxyl mechanism, the conversion of CO_2 to methanol involves the successive formation of the intermediates CHO (formyl), CH_2O (formaldehyde) and CH_3O (methoxy) by a sequential hydrogenation step described by:

$$CH_{y-1}O^* + 2H^* \rightarrow CH_yO^* + H^*$$

In order to check the effect of water on this process, we have computed this reaction energy in which different CH_yO* species are formed ("formation energy") in the

presence/absence of water that we denotate as “wet” and “dry” conditions. Interestingly, we have found that there is a water-mediated stabilization of the CH_yO* species (see Table S1). Indeed, in contrast to what is observed under a dry ambient, for wet conditions all the CH_yO* formation energies are exothermic (see Table S1), with the formation of methoxy intermediates becoming highly favorable (-0.61 eV).

More interestingly, we found that the presence of water in the system also facilitates the subtraction of the O atom from these species giving CH_y* intermediates. We consider the general equations in “dry” and “wet” atmosphere:

$$\text{Dry: } CH_yO^* \rightarrow CH_y^* + O^*$$

$$\text{Wet: } CH_yO^* + H_2O^* \rightarrow CH_y^* + 2\ OH^*$$

The energies associated with these deoxygenation processes (“deoxygenation energies”) at the Pt/CeO_x interface are included in Table S2 (see also Figures S5-S7 for the corresponding structures).

That water makes easier the extraction of the O atom from the CH_yO groups is due to the interaction with hydrogen atoms and further H shift that leads to the formation of two OH* groups. At the same time, we observe that the deoxygenation is energetically favored as the number of H’s bonded to the C atom (*y*) increases, the transformation of methoxy in methyl (-0.58 eV) being the most favorable process. Therefore, water facilitates the formation of CH_3* species adsorbed on the Pt particle. Likely the large CH peak observed in the C 1s AP-XPS spectra (Figure 3) corresponds to these species. These methyl groups can subsequently react with other radical species produced on the reaction to form a C-C bond and, finally, ethanol. Therefore, water facilitates the formation of CH_3* species and, at the same time, it is making easier further evolution to a higher alcohol. This is

coherent with the fact that the ratio of ethanol respect to methanol is larger in the presence of water (see Figure 2).

E. Reaction paths in the presence of water

After describing the different pathways in which water facilitates the activity/selectivity of the $Pt/CeO_x/TiO_2$ system, the full path from CO_2 hydrogenation to methanol/ethanol in the presence of water is considered. The general paths are shown in Figure 8. The optimized structures for the main steps of the synthesis paths are shown in Figures 9 and 10 (only the main intermediates), and Figures S8 and S9 (all the main steps). Discussion 2 in Supporting Information shows a full description of the synthesis paths. To follow the full path step by step we recommend to reader to have at hand at the same time the figures 8, S8 and S9, and to read the Discussion 2 in the Supporting Information. As seen in Figures 9 and 10, the binding and transformation of CO_2 into methanol or ethanol is carried out by platinum and cerium atoms perturbed by their interaction with titania. The ceria in this interface has structural and electronic properties not seen for bulk ceria.[12,13,38] Here, it is interesting to point out three general things:

(i) While in the methanol synthesis path all the energy barriers are below 1 eV (around 0.5-0.6 eV), in the ethanol synthesis path we found some barriers above 1 eV, mainly related to the O extraction from CH_3O (methoxy) to give CH_3 surface groups and to induce C-C bond formation in the reaction of H_2CO (formaldehyde) with CH_3 to give CH_3CH_2O (ethoxy). This is consistent with the higher amount of methanol over ethanol experimentally observed (Figure 2).

(ii) There is a crossroad at step 20, where the methoxy intermediate is already formed. The two possibilities opened by that crossroad have both a high energy cost: (a) the complete evolution to methanol involves 2.20 eV, (b) the reaction of CH_3O* with H_2O* to give CH_3* and 2 OH* groups (opening the path to ethanol) has an energy barrier of 1.68 eV. In any case, at step 20 the system has enough energy to overcome them because a total of 3.49 eV has been liberated in the previous steps. Therefore, the reactivity of methoxy CH_3O* is the critical step to selectivity since it is the crossroad between the methanol and ethanol synthesis paths. As mentioned previously, the presence of water significantly facilitates the O extraction from CH_3O*, opening the evolution to ethanol.

(iii) The steps 0-20 (CH_3O* formation) are common for the methanol/ethanol synthesis paths.

Of course, this is a schematic representation for only one of the possible pathways that would lead to the ethanol formation, but the associated energy calculations indicate that the whole process is exothermic by -3.25 eV. Also, although some of the barriers are relatively high, the system has enough energy to overcome them. All over this description, one can see the unique properties of the $Pt/CeO_x/TiO_2(110)$ system together with the outstanding collaboration of water in the formation of methanol and ethanol. In agreement with the experimental data in Figures 2 and 3, the theoretical calculations show that water can have a strong effect on the chemistry associated with the hydrogenation of CO_2, modifying the conversion and selectivity.

A review of the existing literature for CO_2 hydrogenation indicates that the performance of a metal/oxide catalyst can depend on the size of the metal and oxide

components (nano vs bulk) and the possible existence of strong metal-support interactions that can modify the intrinsic catalytic properties of the metal and oxide.[3,8,9,58,59,60] In the $Pt/CeO_x/TiO_2(110)$ system examined above, the interface combines small nanoparticles of platinum and ceria modified by interactions with titania. This is a unique system. Thus, small and large particles of Pt deposited on surfaces of pure bulk titania or pure bulk ceria do not match the production of methanol and ethanol seen on $Pt/CeO_x/TiO_2$ (Figure 2). In previous studies, we have found that the catalytic behavior seen for $metal/CeO_x/TiO_2(110)$ surfaces in batch reactors can be transferred to powder systems and flow reactors if the $metal\text{-}CeO_x\text{-}TiO_2$ interface remains present.[61,62] As shown in the DFT and XPS studies, each component of the interface plays a specific role in the binding and conversion of CO_2 and, thus, such motif must be present in any technical catalysts.[63] On powders of titania, it is possible to deposit different structures of ceria: Isolated clusters, chains, small two-dimensional sheets, and three-dimensional particles. On top of these CeO_x/TiO_2 powder systems, one can disperse small amounts of platinum to generate $Pt\text{-}CeO_x\text{-}TiO_2$ interfaces.[64,65]

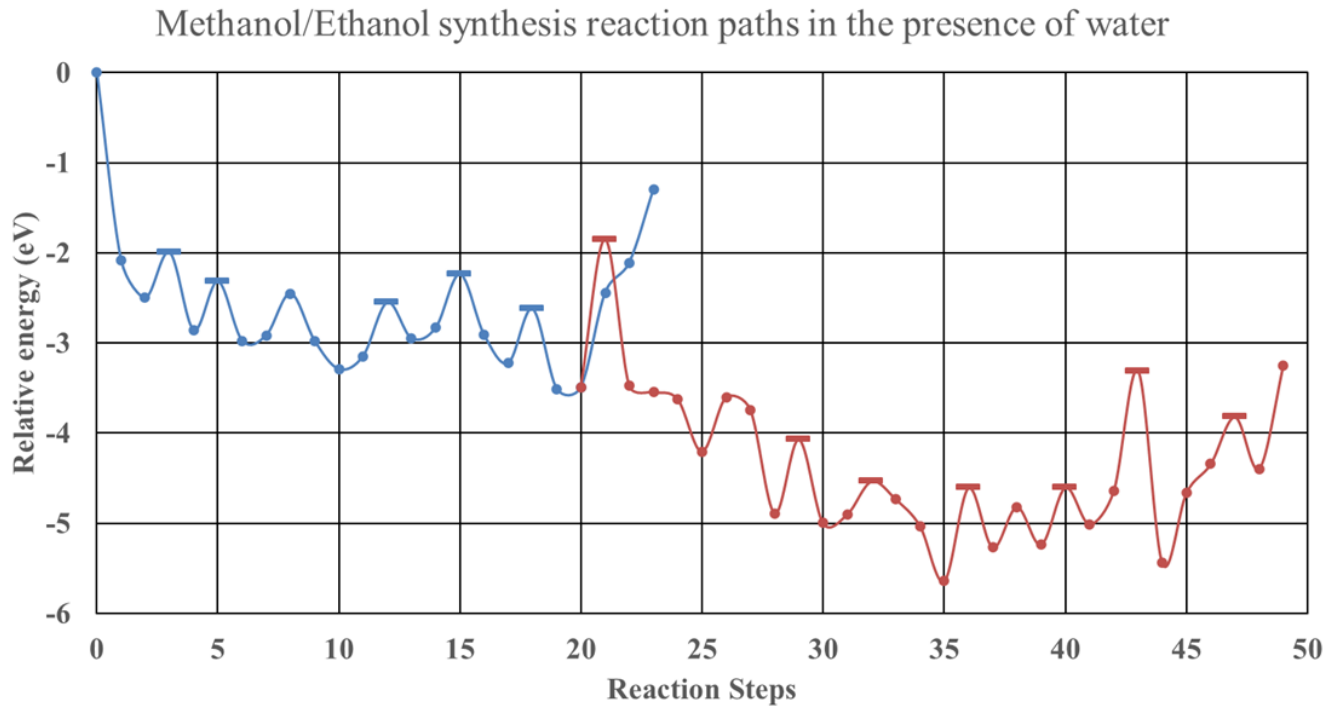

Step	State
0	H_2O^* + 2 CO_2 (g) + 6 H_2(g)
1	H_2O^* + CO_2^* + CO_2 (g) + 6 H_2(g)
2	H_2O^* + CO_2^* + 2 H*Pt + CO_2 (g) + 5 H_2(g)
3	TS
4	H_2O^* + OCOH* + H*Pt + CO_2 (g) + 5 H_2(g)
5	TS
6	H_2O^* + CO* + OH* + H*Pt + CO_2 (g) + 5 H_2(g)
7	2 H_2O^* + CO* + CO_2 (g) + 5 H_2(g)
8	H_2O^* + CO* + CO_2 (g) + 5 H_2(g) + H_2O(g)
9	H_2O^* + CO* + 2 H*Pt + CO_2 (g) + 4 H_2(g) + H_2O(g)
10	H* + OH* + CO* + 2 H*Pt + CO_2 (g) + 4 H_2(g) + H_2O(g)
11	H* + OH* + CO* + 2 H*Pt' + CO_2 (g) + 4 H_2(g) + H_2O(g)
12	TS
13	HCO* + OH* + H* + H*Pt + CO_2 (g) + 4 H_2(g) + H_2O(g)
14	HCO* + OH* + H* + H*Pt' + CO_2 (g) + 4 H_2(g) + H_2O(g)
15	TS
16	H_2CO^* + OH* + H* + CO_2 (g) + 4 H_2(g) + H_2O(g)
17	H_2CO^* + OH* + H* + 2 H*Pt + CO_2 (g) + 3 H_2(g) + H_2O(g)
18	TS
19	CH_3O^* + OH* + H* + H*Pt + CO_2 (g) + 3 H_2(g) + H_2O(g)
20	CH_3O^* + H_2O^* + H*Pt + CO_2 (g) + 3 H_2(g) + H_2O(g)
21	CH_3O^*Pt + H_2O^* + H*Pt + CO_2 (g) + 3 H_2(g) + H_2O(g)
22	CH_3OH^*Pt + H_2O^* + CO_2 (g) + 3 H_2(g) + H_2O(g)
23	H_2O^* + CO_2 (g) + 3 H_2(g) + H_2O(g) + CH_3OH(g)

Step	State
20	CH_3O^* + H_2O^* + H*Pt + CO_2 (g) + 3 H_2(g) + H_2O(g)
21	TS
22	CH_3^* + 2 OH* + H*Pt + CO_2 (g) + 3 H_2(g) + H_2O(g)
23	CH_3^*' + 2 OH* + H*Pt + CO_2 (g) + 3 H_2(g) + H_2O(g)
24	CH_3^*' + OH* + H_2O^* + CO_2 (g) + 3 H_2(g) + H_2O(g)
25	CH_3^*' + OH* + H_2O^* + 2 H*Pt + CO_2 (g) + 2 H_2(g) + H_2O(g)
26	CH_3^*' + 2 H_2O^* + H*Pt + CO_2 (g) + 2 H_2(g) + H_2O(g)
27	CH_3^*' + H_2O^* + H*Pt + CO_2 (g) + 2 H_2(g) + 2 H_2O(g)
28	CH_3^*' + H_2O^* + H*Pt + CO_2^* + 2 H_2(g) + 2 H_2O(g)
29	TS
30	CH_3^*' + H_2O^* + COOH* + 2 H_2(g) + 2 H_2O(g)
31	CH_3^*' + H_2O^* + COOH*' + 2 H_2(g) + 2 H_2O(g)
32	TS
33	CH_3^*' + H_2O^* + CO* + OH* + 2 H_2(g) + 2 H_2O(g)
34	CH_3^*' + H_2O^* + 2 H*Pt + CO* + OH* + H_2(g) + 2 H_2O(g)
35	CH_3^*' + 2 H_2O^* + H*Pt + CO* + H_2(g) + 2 H_2O(g)
36	TS
37	CH_3^*' + 2 H_2O^* + HCO* + H_2(g) + 2 H_2O(g)
38	CH_3^*' + H_2O^* + HCO*' + H_2(g) + 3 H_2O(g)
39	CH_3^*' + H_2O^* + 2 H*Pt + HCO*' + 3 H_2O(g)
40	TS
41	CH_3^*' + H_2O^* + H*Pt + H_2CO^* + 3 H_2O(g)
42	CH_3^*'' + H_2O^* + H*Pt + H_2CO^* + 3 H_2O(g)
43	TS
44	$CH_3CH_2O^*$ + H_2O^* + H*Pt + 3 H_2O(g)
45	$CH_3CH_2O^*$Pt + H_2O^* + H*Pt + 3 H_2O(g)
46	$CH_3CH_2O^*$Pt' + H_2O^* + H*Pt' + 3 H_2O(g)
47	TS
48	$CH_3CH_2OH^*$Pt + H_2O^* + 3 H_2O(g)
49	H_2O^* + 3 H_2O(g) + CH_3CH_2OH(g)

Figure 8. Reaction paths for methanol/ethanol synthesis. Top: Methanol (blue line) and ethanol (blue and red lines) synthesis reaction paths in the presence of water. Significative transition states are depicted as little horizontal lines. The optimized structures corresponding to the main steps are shown in Figures 9 and 10. The state corresponding to each step of the path are shown in the tables at bottom left (methanol) and bottom right (ethanol). **Bottom left**: Table containing the states of the system in each step of the methanol synthesis reaction path. Table color code: black (gaseous reagents), green (adsorbed species), red (main intermediates), blue (gaseous products). An adsorbed species is indicated by an asterisk. A prime indicates a change in the adsorption position. An asterisk followed by Pt indicates that the adsorption is on the Pt particle. "TS" stands for "transition state". **Bottom right**: Table containing the states of the system in each step of the ethanol synthesis reaction path. Color code: same than bottom left.

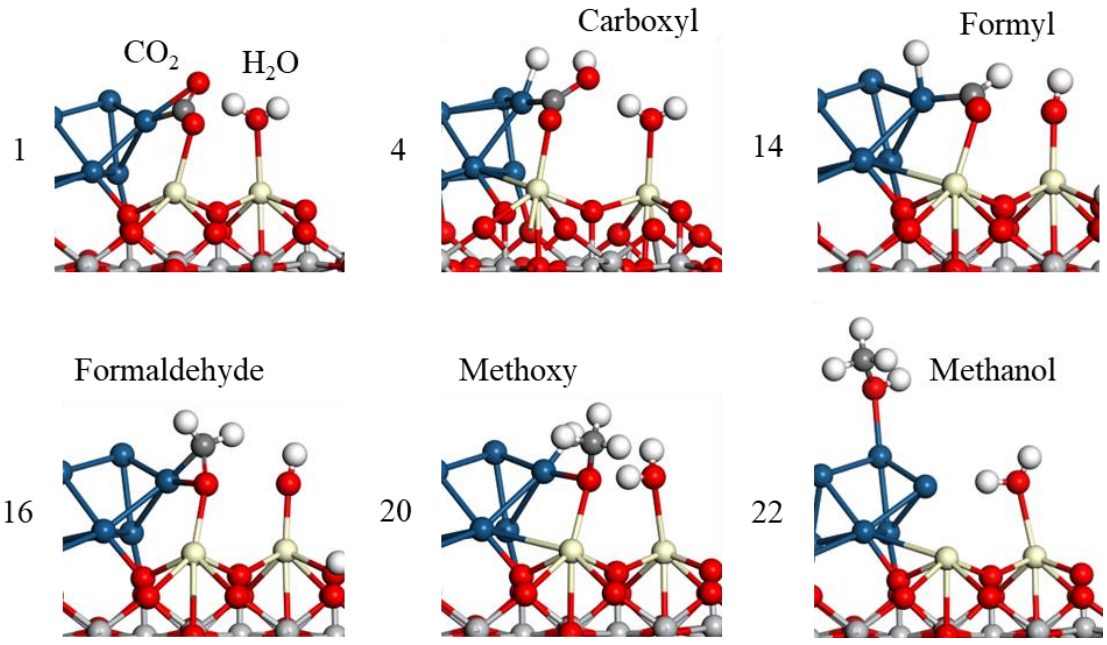

Figure 9. Several optimized structures corresponding to the main intermediates in the methanol synthesis path in the presence of water (numbers correspond to the steps in Figures 8 top and bottom left). Color code: Pt (blue), O (red), Ti (gray), Ce (cream), H (white).

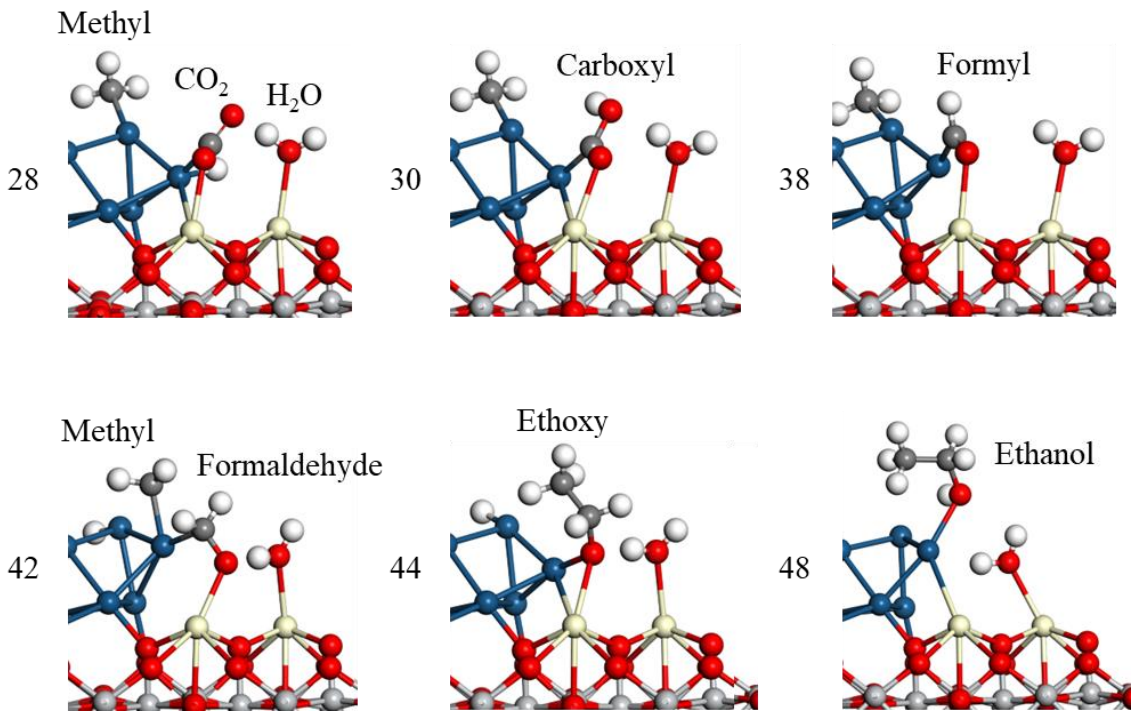

Figure 10. Some optimized structures corresponding to the main intermediates in the ethanol synthesis path in the presence of water (numbers correspond to the steps in Figure 8 top and bottom right). Color code: Pt (blue), O (red), Ti (gray), Ce (cream), H (white).

Conclusions

The results of kinetic experiments and AP-XPS data, together with DFT calculations, reveal that Pt and CeO_x nanoparticles deposited on a TiO_2(110) substrate produce a platinum-ceria-titania interface that exhibits a remarkable surface chemistry for the synthesis of alcohols through CO_2 hydrogenation. From the onset, due to its configuration and electronic properties, this interface shows an outstanding ability to activate CO_2 not seen in typical Cu-ZnO catalysts. The easiness of such activation reflects the stability of a CO_2-surface anchorage that involves formation of Pt-C and C-O-Ce bonds.

The $Pt/CeO_x/TiO_2$ system is an excellent catalyst for the hydrogenation of CO_2 to methanol with even a small amount of ethanol being produced. The results of AP-XPS, corroborated by DFT calculations, indicate that the active state of the catalyst under CO_2 + H_2 reaction conditions consists of a mixture of Ti^{4+}, Ti^{3+}, Ce^{3+}, Pt^0 and, Pt^+, the later exclusively located on the layer in contact with the metal oxide. The addition of small quantities of water vapor significantly enhances the surface coverages of C-containing species (CH_3O, HCOO, CO_3, CH_x) and alcohol production. Although both methanol and ethanol production are improved, the presence of water preferentially raises the ethanol yield. The EtOH/MeOH ratio is always < 1, but it almost doubles in the presence of water.

The DFT simulations strongly suggest that the mechanism that leads to methanol formation follows a pathway through a CH_3O species, and that it is only plausible when Ce^{3+} and Pt are present. Here, the special electronic properties of ceria in contact with titania are important. The calculations also show that the presence of water increases the CO_2-support interaction and facilitates the hydrogenation of CO_2 favoring the formation of the key intermediate CH_3O at the Pt/CeOx interface. Likewise, adsorbed water molecules help its full deoxygenation to form CH_3 species on Pt, facilitating the path to ethanol production. The theoretical modeling of the whole paths to methanol and ethanol in the presence of water indicates that the CH_3O species are precisely at the crossroad to methanol/ethanol synthesis.

Associated Content

Supporting information

Additional AP-XPS spectra for the interaction of CO_2, CO_2/H_2 and $CO_2/H_2/H_2O$ with $Pt/CeOx/TiO_2$ surfaces. DFT calculated structures and energy changes for the reaction of $CO_2/H_2/H_2O$ with $Pt/CeOx/TiO_2$. Detailed discussion of some key facts in the mechanisms for CO_2 activation and hydrogenation.

Acknowledgements

This work was supported by the U.S. Department of Energy, Office of Science, Office of Basic Energy Sciences, and Catalysis Science Program under contract No. DE-SC0012704. The authors are grateful to J.B. Park and J. Hrbek for their help with the STM images. S. Luo helped with preliminary studies of AP-XPS. The work done at the University of Sevilla was funded by the Spanish Ministerio de Ciencia e Innovación, grant number PID2019-106871GB-I00. This research used resources of the 23-ID-2 (IOS) beamline of the National Synchrotron Light Source II, a U.S. Department of Energy (DOE) Office of Science User Facility operated for the DOE Office of Science by Brookhaven National Laboratory under Contract No. DE-SC0012704.

References

[1] Anderson, T. R.; Hawkins, E.; Jones, P. D., CO_2, the greenhouse effect and global warming: from the pioneering work of Arrhenius and Callendar to today's Earth System Models. *Endeavour* **2016,** *40*, 178-187

[2] Aresta, M. Carbon Dioxide as Chemical Feedstock; Wiley-VCH, New York, 2010

[3] Porosoff, M. D.; Yan, B.; Chen, J. G. Catalytic reduction of CO_2 by H_2 for synthesis of CO, methanol and hydrocarbons: challenges and opportunities. *Energy Environ. Sci.* **2016**, *9*, 62−73.

[4] Schumann, J.; Tarasov, A.; Thomas, N.; Schlögl, R.; Behrens, M. Cu,Zn-based catalyst for methanol synthesis: On the effect of calcination conditions and the part of residual carbonates. *Applied Catalysis A* **2016**, *516*, 117-123.

[5] Laudenschleger, D.; Ruland, H.; Muhler, M. Identifying the nature of the active sites in methanol synthesis over $Cu/ZnO/Al_2O_3$ catalysts. *Nat Commun* **2020**, *11***,** 3898.

[6] Beck, A. ; Zabilskiy, M. ; Newton, M.A. ; Safonova, O. ; Willinger, M.G. ; van Bokhoven, J.A. Following the structure of copper-zinc-alumina across the pressure gap in carbon dioxide hydrogenation. *Nat Catal* **2021**, *4***,** 488–497.

[7] Behrens, M.; Studt, F.; Kasatkin, I.; Kuhl, S.; Havecker, M.; Abild-Pedersen, F.; Zander, S.; Girgsdies, F.; Kurr, P.; Kniep, B. L.; Tovar, M.; Fischer, R. W.; Norskov, J. K.; Schlogl, R. The Active Site of Methanol Synthesis over $Cu/ZnO/Al_2O_3$ Industrial Catalysts, *Science* **2012**, *336*, 893-897.

[8] Subramani, V.; Gangwal, S. K. A Review of Recent Literature to Search for an Efficient Catalytic Process for the Conversion of Syngas to Ethanol, *Energy & Fuels* **2008**, *22*, 814-839.

[9] Spivey, J. J.; Egbebi, A. Heterogeneous catalytic synthesis of ethanol from biomass-derived syngas, *Chemical Society Reviews* **2007**, *36*, 1514-1528.

[10] Wang, X.; Ramírez, P.J.; Liao, W.; Rodriguez, J.A.; Liu. P. Cesium-Induced Active Sites for C–C Coupling and Ethanol Synthesis from CO_2 Hydrogenation on $Cu/ZnO(000\bar{1})$ Surfaces, *J. Am. Chem. Soc.* **2021**, *143*, 13103-13112.

[11] Grinter, D.C.; Graciani, J.; Palomino, R.M.; Xu, F.; Waluyo, I.; Fdez Sanz, J.; Senanayake, S.D.; Rodriguez, J.A. Adsorption and Activation of CO_2 on $Pt/CeO_x/TiO_2(110)$: Role of the Pt-CeO_x Interface, *Surf. Sci.* **2021**, *710*, 121852.

[12] Park, J. B.; Graciani, J.; Evans, J.; Stacchiola, D.; Senanayake, S. D.; Barrio, L.; Liu, P.; Sanz, J. F.; Hrbek, J.; Rodriguez, J. A. Gold, Copper, and Platinum Nanoparticles Dispersed on $CeO_x/TiO_2(110)$ Surfaces: High Water-Gas Shift Activity and the Nature of the Mixed-Metal Oxide at the Nanometer Level, *J. Am. Chem. Soc.* **2010**, *132*, 356-363.

[13] Park, J. B.; Graciani, J.; Evans, J.; Stacchiola, D.; Ma, S.; Liu, P.; Nambu, A.; Sanz, J. F.; Hrbek, J.; Rodriguez, J. A. High Catalytic Activity of $Au/CeO_x/TiO_2(110)$ Controlled by the Nature of the Mixed-metal Oxide at the Nanometer Level, *Proceedings of the National Academy of Sciences* **2009**, *106*, 4975-4980

[14] Palomino, R.M.; Ramirez, P.J.; Liu, Z.; Hamlyn, R.; Waluyo, I.; Mahapatra, M.; Orozco, I.; Hunt, A.; Simonovis, J.P.; Senanayake, S.D.; Rodriguez, J.A. Hydrogenation of CO_2 on ZnO/Cu(100) and ZnO/Cu(111) Catalysts: Role of Copper Structure and Metal-Oxide Interface in Methanol Synthesis, *J. Phys. Chem. B*, **2018**, *122*, 794-800.

[15] Kattel, S.; Ramírez, P. J.; Chen, J. G.; Rodriguez, J. A.; Liu, P., Active Sites for CO_2 Hydrogenation to Methanol on Cu/ZnO Catalysts. *Science* **2017**, *355*, 1296-1299.

[16] Yoshihara, J.; Campbell, C.T. Methanol Synthesis and Reverse Water–Gas Shift Kinetics over Cu(110) Model Catalysts: Structural Sensitivity. *J. Catal*. **1996**, *161*, 776-783.

[17] Kresse, G.; Joubert, J. From Ultrasoft Pseudopotentials to the Projector Augmented-Wave Method, *Phys. Rev. B* **1999**, *59*, 1758-1775.

[18] P. E. Blöchl, P. E. Projector Augmented-Wave Method, *Phys. Rev. B* **1994**, *50*, 17953-17979.

[19] Perdew, J.; Chevary, J.; Vosko, S.; Jackson, K.; Pederson, M.; Singh, D.; Fiolhais, C. Atoms, Molecules, Solids, and Surfaces – Applications of the Generalized Gradient Approximation for Exchange and Correlation, *Phys. Rev. B* **1992**, *46*, 6671-6687.

[20] Kresse, G.; Hafner, J. Ab-initio Molecular-Dynamics for Liquid-Metals, *Phys. Rev. B* **1993**, *47*, 558- 561.

[21] Kresse, G.; Furthmuller, J. Efficiency of Ab-initio Total Energy Calculations for Metals and Semiconductors Using a Plane-Wave Basis Set, *Comput. Mater. Sci.* **1996**, *6*, 15-50.

[22] Marquez, A. M.; Plata, J. J.; Fdez. Sanz, J. Role of Coverage and Surface Oxidation Degree in the Adsorption of Acetone on TiO_2 (110). A Density Functional Study, *J. Phys. Chem. C* **2009**, *113*, 19973-19980.

[23] Plata, J. J.; Graciani, J.; Evans, J.; Rodriguez, J. A.; Sanz, J. F. Cu Deposited on CeOx-Modified TiO_2 (110): Synergistic Effects at the Metal-Oxide Interface and the Mechanism of the WGS Reaction, *ACS Catal.* **2016**, *6*, 4608- 4615.

[24] Dudarev, S. L.; Botton, G. A.; Savrasov, S. Y.; Humphreys, C. J.; Sutton, A. P. Electron-Energy-Loss Spectra and the Structural Stability of Nickel Oxide: An LSDA+U Study, *Phys. Rev. B* **1998**, *57*, 1505-1509.

[25] Fabris, S.; de Gironcoli, S.; Baroni, S.; Vicario, G.; Balducci, G. Reply to Comment on 'Taming Multiple Valency with Density Functionals: A Case Study of Defective Ceria', *Phys. Rev. B* **2005**, *72*, 237102.

[26] Cococcioni, M.; de Gironcoli, S. Linear Response Approach to the Calculation of the Effective Interaction Parameters in the LDA+U Method, *Phys. Rev. B* **2005**, *71*, 035105.

[27] Castleton, C. W. M.; Kullgren, J.; Hermansson, K. Tuning LDA+U for Electron Localization and Structure at Oxygen Vacancies in Ceria, *J. Chem. Phys.* **2007**, *127*, 244704.

[28] Andersson, D. A.; Simak, S. I.; Johansson, B.; Abrikosov, I. A.; Skorodumova, N. V. Modeling of CeO_2, Ce_2O_3, and CeO_{2-x} in the LDA Plus U Formalism, *Phys. Rev. B* **2007**, *75*, 035109.

[29] Nolan, M.; Grigoleit, S.; Sayle, D. C. Density Functional Theory Studies of the Structure and Electronic Structure of Pure and Defective Low Index Surfaces of Ceria, *Surf. Sci.* **2005**, *576*, 217-229.

[30] Nolan, M.; Parker, S. C.; Watson, G. W. The Electronic Structure of Oxygen Vacancy Defects at the Low Index Surfaces of Ceria, *Surf. Sci.* **2005**, *595*, 223-232.

[31] Nolan, M.; Parker, S. C.; Watson, G. W. Reduction of NO_2 on Ceria Surfaces, *J. Phys. Chem. B* **2006**, *110*, 2256-2262.

[32] Watkins, M. B.; Foster, A. S.; Shluger, A. L. Hydrogen Cycle on CeO_2 (111) Surfaces: Density Functional Theory Calculations, *J. Phys. Chem. C* **2007**, *111*, 15337-15341.

[33] Yang, Z.; Lu, Z.; Luo, G. First-Principles Study of the Pt/CeO_2(111) Interface, *Phys. Rev. B* **2007**, *76*, 075421.

[34] Da Silva, J. L. F. Stability of the Ce_2O_3 Phases: A DFT+U Investigation, **Phys. Rev. B 2007**, *76*, 193108.

[35] Da Silva, J. L. F.; Ganduglia-Pirovano, M. V.; Sauer, J.; Bayer, V.; Kresse, G. Hybrid Functionals Applied to Rare-Earth Oxides: The Example of Ceria, *Phys. Rev. B* **2007**, *75*, 045121.

[36] Loschen, C.; Carrasco, J.; Neyman, K. M.; Illas, F. First-Principles LDA Plus U and GGA Plus U Study of Cerium Oxides: Dependence on the Effective U Parameter, *Phys. Rev. B* **2007**, *75*, 035115.

[37] Loschen, C.; Migani, A.; Bromley, S. T.; Illas, F.; Neyman, K. M. Density Functional Studies of Model Cerium Oxide Nanoparticles, *Phys. Chem. Chem. Phys.* **2008**, *10*, 5730-5738.

[38] Graciani, J.; Plata, J. J.; Fdez Sanz, J.; Liu, P.; Rodriguez, J. A. A Theoretical Insight into the Catalytic Effect of a Mixed-metal Oxide at the Nanometer Level: The Case of the Highly Active Metal/CeO_x/TiO_2(110) Catalysts, *J. Chem. Phys.* **2010**, *132*, 104703.

[39] Henkelman, G.; Uberuaga, B.; Jonsson, H. A climbing image nudged elastic band method for finding saddle points and minimum energy paths *J. Chem. Phys.* **2000**, *113*, 9901-9904.

[40] Bruix, A.; Rodriguez, J.A.; Ramirez, P.; Senanayake, S.D.; Evans, J.; Park, J.B.; Stacchiola, D.; Liu, P.; Hrbek, J.; Illas, F. A New Type of Metal-Support Interaction and the Production of H_2 through the Transformation of Water on Pt/CeO_2(111) and Pt/CeO_x/TiO_2(110) Catalysts, *J. Am. Chem. Soc.* **2012**, *134*, 8968-8974.

[41] Huang, E.; Orozco, I.; Ramirez, P.J.; Liu, Z.; Zhang, F.; Mahapatra, M.; Nemsak, S.; Senanayake, S.; Rodriguez, J.A.; Liu, P. Selective Methane Oxidation to Methanol on

ZnO/Cu_2O/Cu(111): Multiple Site-Dependent Behaviors, *J. Am. Chem. Soc*. **2021**, *143*, 19018-19032.

[42] Rui, N.; Huang, E,; Kim, J.; Mehar, V.; Shi, R.; Rosales, R.; Tian, Y.; Hunt, A.; Waluyo, I.; Senanayake, S.D.; Liu, P.; Rodriguez, J.A. CO_2 Hydrogenation to Methanol over Inverse ZrO_2/Cu(111) Catalysts: The Fate of Methoxy under Dry and Wet Conditions, *J. Phys. Chem. C*, **2022**, *126*, 14479-14486.

[43] Rodriguez, J.A.; Rui, N.; Zhang, F.; Senanayake, S.D. In Situ Studies of Methane Activation Using Synchrotron-Based Techniques: Guiding the Conversion of C-H Bonds, *ACS Catal.* **2022**, *12*, 5470-5488.

[44] Butcher, D.R.; Grass, M.E.; Zeng, Z.; Aksoy, F.; Bluhm, H.; Li, W.-X.; Mun, B.S,; Somorjai, G.A.; Liu, Z. In Situ Oxidation Study of Pt(110) and its Interaction with CO, *J. Am. Chem. Soc.* **2011**, *133*, 20319-20325,

[45] Albretcht, P. Jiang, D.; Mullins, D.R, CO_2 Adsorption As a Flat-Lying, Tridentate Carbonate on CeO_2(100), *J. Phys, Chem. C*, **2014**, *118*, 9042-9050.

[46] Senanayake, S.D.; Ramirez, P.J.; Waluyo, I.; Kundu, S.; Mudiyanselage, K.; Liu, Z.; Liu, Z.; Axnanda, S.; Stacchiola, D.J.; Evans, J.; Rodriguez, J.A., Hydrogenation of CO_2 to Methanol on CeO_x/Cu(111) and ZnO/Cu(111) Catalysts: Role of the Metal–Oxide Interface and Importance of Ce^{3+} Sites, *J. Phys. Chem. C*, **2016**, *120*, 1778-1784.

[47] Kim, K.S.; Barteau, M.A. Reaction of Methanol on TiO_2(001) Single Crystal Surfaces, *Surf. Sci.* **1989**, *223*, 13-32.

[48] Yuan, Q,; Wu, Z.; Jin, Y.; Xu, L.; Xiong, F.; Ma, Y.; Huang, W. Photocatalytic Cross-coupling of Methanol and Formaldehyde on a Rutile TiO_2(110) Surface, *J. Am. Chem. Soc.* **2013**, *135*, 5212-5219.

[49] Mullins, D.R.; Robbins, M.D.; Zhou, J. Adsorption and Reaction of Methanol on Thin-film Cerium Oxide, *Surf. Sci.* **2006**, *600*, 1547-1558.

[50] Vohs, J.M.; Barteau, M.A. Conversion of Methanol, Formaldehyde and Formic Acid on the Polar Faces of Zinc Oxide, *Surf. Sci.* **1986**, *176*, 91-114.

[51] David, R.B.; Yaacov, A.B.; Head, A.R.; Eren, B. Methanol Decomposition on Copper Surfaces under Ambient Conditions: Mechanism, Surface Kinetics, and Structure Sensitivity, *ACS Catal.* **2022**, *12*, 7709-7718.

[52] Hamlyn, R.C.; Mahapatra, M.; Grinter, D.C.; Xu, F.; Luo, S.; Palomino, R.M.; Kattel, S.; Waluyo, I.; Liu, P.; Stacchiola, D,J,; Senanayake, S.D.; Rodriguez, J.A. Imaging the ordering of a weakly adsorbed two-dimensional condensate: ambient-pressure microscopy and spectroscopy of CO_2 molecules on rutile TiO_2(110), *Phys. Chem. Chem. Phys.* **2018**, 20, 13122-13126.

[53] Chen, S.; Xiong, F.; Huang, W. Surface chemistry and catalysis of oxide model catalysts from single crystals to nanocrystals, *Surface Science Reports* **2019**, *74*, 100471.

[54] Fernández-Torre, D.; Carrasco, J.; Ganduglia-Pirovano, M.V.; Pérez, R. Hydrogen Activation, Diffusion and Clustering on CeO_2(111): A DFT+U study. *J. Chem. Phys.* **2014**, *141*, 014703.

[55] García-Melchor, M.; López, N. Homolytic Products from Heterolytic Paths in H_2 Dissociation on Metal Oxides: The Example of CeO_2. *J. Phys. Chem. C* **2014**, *118*, 10921.

[56] Auras, S.V.; van Lent, R.; Bashlakov, D.; Piñeiros Bastidas, J.M.; Roorda, T.; Spierenburg, R.; Juurlink, L.B.F. Scaling Platinum-Catalyzed Hydrogen Dissociation on Corrugated Surfaces. *Angew. Chem. Int. Ed.* **2020**, *59*, 20973.

[57] Koverga, A.A.; Flórez, E.; Jiménez-Ororzco, C.; Rodriguez, J.A. Spot the difference: hydrogen adsorption and dissociation on unsupported platinum and platinum-coated transition metal carbides, *Phys. Chem. Chem. Phys.* **2021**, *23*, 20255.

[58] Vogt, C.; Monai, M.; Sterk, E.R. ; Palle, J. ; Melcherts, A.E.M. ; Zijlstra, B. ; Groeneveld, E.; Berben, P.T.; Boereboom, J.M.; Hensen, E.M.J.; Meiner, F.; Filot, I.A.W.; Weckhuysen, B.M. Understanding Carbon Dioxide Activation over Nickel, *Nature Communications*, **2019**, *10*, 5330.

[59] Parastaev, A.; Muravev, V.; Huertas Osta, E,; Van Hoof, A.J.F.; Kimpel, T.F.; Kosibov, N.; Hensen, E,J.M. Boosting CO_2 Hydrogenation Activity via Size-Dependent Meta-Support Interactions in Cobalt/Ceria Catalysts, *Nature Catal.* **2020**, *3*, 526-533

[60] Rodriguez, J.A.; Liu, P.; Stacchiola, D.J.; Senanayake, S.D.; White, M.G.; Chen, J.G. Hydrogenation of CO_2 to Methanol: Importance of Metal-Oxide and Metal-Carbide Interfaces in the Activation of CO_2. *ACS Catal.* **2015**, *5*, 6696–6706.

[61] Si, R.; Tao, J.; Evans, J.; Park, J.B.; Barrio, L.; Hanson, J.C. Zhu, Y.; Hrbek, J.; Rodriguez, J.A. Effect of Ceria on Gold–Titania Catalysts for the Water–Gas Shift Reaction: Fundamental Studies for Au/CeO_x/TiO_2(110) and Au/CeO_x/TiO_2 Powders, *J. Phys. Chem. C*, **2012**, *116*, 23547-23555.

[62] Rodriguez, J.A.; Senanayake, S.D.; Stacchiola, D.; Liu, P.; Hrbek, J. The Activation of Gold and the Water-gas Shift Reaction: Insights from Studies with Model Catalysts, *Acc. Chem. Res.* **2014**, *47*, 773-782.

[63] Johnston-Peck, A.C.; Senanayake, S.D.; Plata, J.J.; Kundu, S.; Xu, W.; Barrio, L.; Graciani, J.; Sanz, J.F.; Navarro, R.; Fierro, J.L.G.; Stach, E.A.; Rodriguez, J.A. Nature of the Mixed-Oxide Interface in Ceria–Titania Catalysts: Clusters, Chains, and Nanoparticles, *J. Phys. Chem. C*, **2013**, *117*, 14463–14471.

[64] Lai, X.-M.; Xiao, Q. ; Ma, C. ; Wang, W.W. ; Jia, C.-J. Heterostructured Ceria–Titania-Supported Platinum Catalysts for the Water Gas Shift Reaction, *ACS Appl. Mater. Interfaces* **2022**, *14*, 8575–8586.

[65] Kundu, S.; Ciston, J.; Senanayake, S.D.; Arena, D.A.; Fujita, E.; Stacchiola, D.; Barrio, L.; Navarro, R.; Fierro, J.L.G.; Rodriguez, J.A. Exploring the Structural and Electronic Properties of Pt/Ceria-Modified TiO_2 and Its Photocatalytic Activity for Water Splitting under Visible Light, *J. Phys. Chem. C*, **2012**, *116*, 14062–14070.

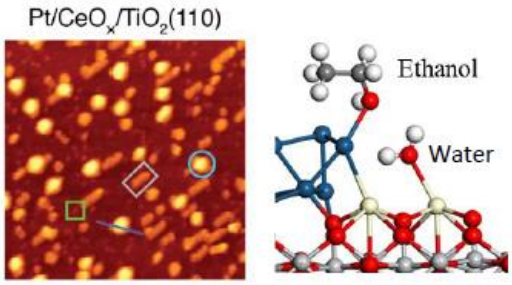

TOC